buildings

MDPI

Article

Analysis of Multi-Stage Slope Displacement and Internal Force of Supporting Structure of Frame Prestressed Anchor Cable Support

Jingbang Li [1,*], Yanpeng Zhu [2], Shuaihua Ye [2,*], Nianxiang Li [2] and Bo Liu [2]

[1] School of Civil Engineering, Lanzhou Institute of Technology, Lanzhou 730050, China
[2] School of Civil and Hydraulic Engineering, Lanzhou University of Technology, Lanzhou 730050, China; zhuyp@lut.edu.cn (Y.Z.); linianxiang55@163.com (N.L.); liubo9981202@163.com (B.L.)
* Correspondence: lijingbang@lzit.edu.cn (J.L.); yesh@lut.edu.cn (S.Y.)

Abstract

Relying on an engineering case, this study establishes an analysis model using PLAXIS 3D and GeoStudio, and compares and analyzes the slope deformation and internal force of the supporting structure with different slope grades and different platform widths at the same height. The results show that the greatest displacement manifests in the lower segments of the slope, which is 12.99 mm, and the maximum anchoring force manifests in the mid-level and lower segments of the slope, which is 288.1 kN. A close correlation is observed between the simulated horizontal displacement of the slope, the maximum axial force of the anchor cable, and the corresponding field measurement results, indicating that the model parameters are satisfactory and that the resulting calculations are reliable. In consideration of the comprehensive stability of the slope, the stability coefficient increased by approximately 1.42% with two-stage slope support and by about 3.48% with four-stage slope support. The axial force of anchor cables was reduced by around 9.5% under two-stage grading, while four-stage grading decreased the maximum axial force of the middle–lower anchors by nearly 27%. The distance between the entrance and exit of the overall sliding surface and the slope surface also decreases with the increase in slope grading and platform width. This study systematically evaluates the combined effects of slope grading, platform width, and frame prestressed anchors. When site conditions permit, slope grading should be prioritized over simply widening the platform, as grading more effectively enhances slope stability and reduces anchor cable loads.

Keywords: frame prestressed anchor; multi-stage slope; slope displacements; internal force analysis

Academic Editor: Eugeniusz Koda

Received: 24 August 2025
Revised: 30 September 2025
Accepted: 9 October 2025
Published: 11 October 2025

Citation: Li, J.; Zhu, Y.; Ye, S.; Li, N.; Liu, B. Analysis of Multi-Stage Slope Displacement and Internal Force of Supporting Structure of Frame Prestressed Anchor Cable Support. *Buildings* **2025**, *15*, 3668. https://doi.org/10.3390/buildings15203668

1. Introduction

In recent years, the instability of high slopes has not only led to substantial casualties and property losses, but also seriously affected the safe operation of infrastructure in construction, transportation, water conservancy, and other fields [1–4]. To ensure the stability of high slopes, the support method of multi-stage slope combined with a frame prestressed anchor cable has been widely used. For the multi-level slope supported by a frame prestressed anchor, the displacement and internal force of the supporting structure are two important indexes to reflect the stability of multi-level slope. In practical engineering, slope classification and platform width at multiple levels have great effect on the overall stability of a slope, slope deformation, and the internal force of supporting

structure. Therefore, investigating the effects of slope series and platform width on slope displacement and the internal forces of supporting structures holds considerable practical significance. With the increasing implementation of multi-level slope projects, numerous domestic and international scholars have carried out related studies on both high- and multi-level slopes [5–11].

Jia [12] analyzed the overall and local stability of a three-stage slope project in a certain area, determined the most dangerous potential sliding surface, calculated the displacement, and explored the effect of different ground motion parameters on slope response. Luo [13] constructed the logarithmic spiral failure limit analysis model of three-stage slopes under the effect of seismic effect, and analyzed the effect of various factors on the stability of multi-stage slopes under seismic effect. Research has demonstrated that the angle of slope and the width of steps are important factors in the stability of multi-stage slopes in the context of seismic activity. Yan [14] took the high slope project of the Miaoling 750 kV substation in the loess hilly area of Ningxia as an example to analyze the upper limit solution of safety factors and the influencing factors, and established the numerical model for the high slope of the project. The results show that the safety factor of the slope changes approximately linearly with the internal friction angle and the step width, and increases first and then stabilizes with the increase in the cohesion ratio. In order to clarify the safety control mechanism of the wide platform on the high cutting slope, Li [15] designed the limit equilibrium method for the 2D working conditions of different width platforms, 1–7 grade slopes, and different wide platform positions, and used the stability analysis to determine the optimal platform width and position. The results show that the safety control of the wide platform for the high cutting slope lies in the blocking mechanism, the energy dissipation mechanism, and the mechanism of reducing sliding resistance and increasing stability, and it is found that a bigger platform width does not mean that it is the better.

At the same time, some scholars have studied the high slope with supporting structures. Jia Zhijie [16] analyzed the stability of the slope under the conditions of having support and no support, combined with actual high slope engineering. The results show that the stress and displacement values without the supporting structure are 1~1.5 times that with the supporting structure. The supporting structure can effectively reduce the risk of thermal melt collapse of the slope and provides a theoretical basis for engineering design. Relying on the unstable slope geological disaster control project of the Guiyang Xiaoguan project, Zhao et al. [17] used a prestressed anchor cable frame beam and anchor frame beam to protect the broken rock and soil on the high slope, discussed the construction technology of anchor cable and anchor rod, put forward the control measures, and analyzed and summarized the reinforcement effect. Based on the unstable slope support project of Baidaoping Shigou in the Chengguan District of Lanzhou City, Zhu et al. [18] collected and summarized the displacement of the supporting structure, the internal force of the pile body, and the monitoring value of the anchor cable prestress, and analyzed the stress of the prestressed anchor cable pile wall in the process of multi-stage slope support in detail. Wang [19] selected a typical section with uneven stratum distribution and weak interlayer in a slope support project in Fengchi Mountain, Leshan City, Sichuan Province, and established a shaking table test model of an unsupported structure and a supporting structure. A series of important conclusions on slope displacement, slope acceleration, and the dynamic response of a supporting structure were obtained. Wang Jiangrong et al. [20] considered soil parameters as random variables, and used the Monte Carlo random sampling method and the limit equilibrium method to calculate the average value of slope stability coefficient, reliability index, and failure probability according to different confidence intervals. The results show that the high cutting slope without a

supporting structure is in a relatively stable and unstable state under natural conditions and rainstorm conditions, respectively, while the cutting slope supported by lattice anchor is in a stable state, which meets the first-level engineering safety standard. Li [21] established a comprehensive three-dimensional automatic monitoring system based on a secondary high slope project of the Zhouqu post-disaster reconstruction project. Through the monitoring and analysis of the internal force and displacement of the slope, some variation characteristics and laws of the slope in the construction and operation stages were found. Based on the GeoStudio2012 analysis software, in the study by Ye [22], a dynamic analysis model was constructed for multi-stage high slopes stabilized with frame prestressed anchors. The investigation focused on the displacement, velocity, acceleration, and axial force responses of the slope during seismic excitation, providing a theoretical basis for evaluating the seismic performance of reinforced multi-level high slopes.

The failure mechanisms and stability of multi-stage slopes are influenced by numerous factors, and the interactions among different slope levels further increase the complexity of their behavior. Despite this, most existing studies have mainly concentrated on the stability of slope soils, paying limited attention to the combined effects of slope grading, platform width, and prestressed anchor cables. Addressing this research gap, it becomes necessary to investigate the stability of multi-stage slopes supported by frame prestressed anchors, which can provide both theoretical insights and practical guidance for improving slope stability and enhancing disaster prevention performance.

2. Project Profile

This slope extends up to 344.5 m in length, and the lithology characteristics of each layer of soil are mainly as follows: ① silty clay with a thickness of 0.5~37 m; ② strongly weathered phyllite, purple black, layered, highly weathered, full-length range of excavation revealed, and almost no vegetation coverage on the slope; the exploration of the maximum depth did not reveal the presence of groundwater. The soil parameters are illustrated in Table 1.

Table 1. Slope soil parameters.

Sample Name	Coefficient of Friction	Angle of Internal Friction /°	Bond Strength /kPa
Silty clay	0.23	25.4	17.4
Strongly weathered phyllite	0.69	34.6	100

The safety level of the slope engineering design is considered as the first level, and the slope toe is equipped with a 3 m high masonry slope protection. The northern slope and the southern slope are supported by the frame prestressed anchor cable structure. The horizontal and vertical spacing of the prestressed anchor cable is 3 m; the inclination angle of the prestressed anchor cable is 20°; and the prestress is 230 kN. The length of the southern slope to be treated is 75 m; the height of the slope to be treated is between 9 m and 39 m; and the slope of the slope to be treated is between 51° and 69°. The design elevation of the southern slope is illustrated in Figure 1.

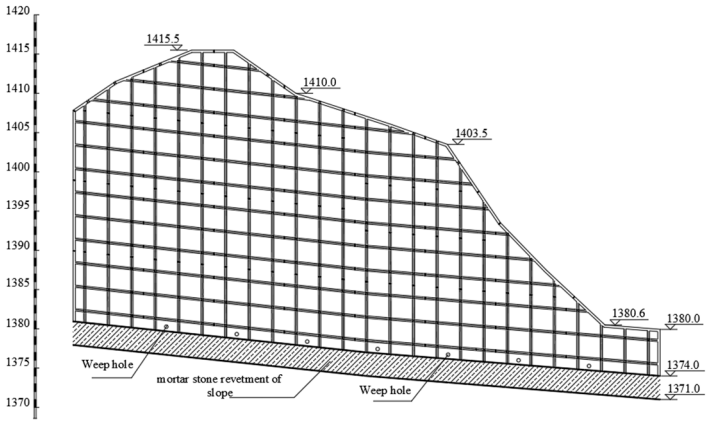

Figure 1. Design elevation diagram of south slope (unit: m).

3. In Situ Monitoring Test

3.1. Design of Monitoring Test Scheme

The construction conditions of the slope form the foundation for this study. The JMDL-3210A displacement meter was adopted on site, with a measurement range of 500 kN and a sensitivity of 0.1 kN. Combined with the design scheme, the section with great hazard in the southern slope is selected for sensor layout. The slope displacement and anchor cable prestress are two important monitoring contents of this test.

3.1.1. Slope Displacement Monitoring Scheme Design

In this test, a single-point displacement meter was used to monitor the slope displacement. Along the monitored section, 12 rows of anchor cables were installed. Displacement meters were arranged at the 3rd, 6th, 8th, and 12th rows of anchor heads, denoted as W1–W4. The location of the displacement meter is illustrated in Figure 2.

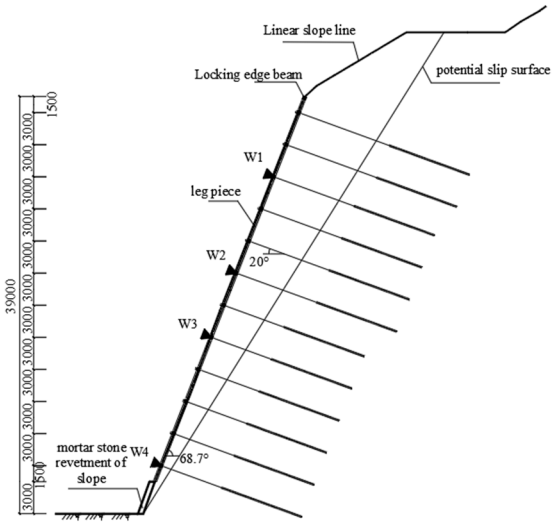

Figure 2. Sensor placement position profile diagram (unit: mm).

3.1.2. Design of Anchor Cable Prestress Monitoring Scheme

In the test, the prestress in the anchor cables within the supporting structure is monitored in real time using an anchor cable dynamometer. In the experiment, anchor cable dynamometers were installed on the 2nd, 4th, 6th, 8th, 10th, and 12th rows of the anchor cables along the monitoring section. The layout position is illustrated in Figure 2.

3.1.3. Wireless Data Acquisition and Transmission Scheme Design

In this test, the data wireless acquisition and transmission system is used to connect the wires of all sensors to the data acquisition module of the system to realize real-time monitoring of the displacement and anchorage force of the anchor cable. The field test photos are illustrated in Figure 3.

(**a**) (**b**)

Figure 3. Field work: (**a**) on-site installation of metal-connecting rod; (**b**) the installation of displacement electric probe is completed.

3.2. Analysis of Monitoring Data

Processed and analyzed, the monitoring data reveals that the deformation of the slope and anchor cable anchoring force can be tracked in real time, thereby assessing the slope stability during the operation stage.

3.2.1. Slope Displacement Analysis

The test uses a single-point displacement meter to monitor the deformation of the slope surface. As illustrated by Figure 3 the four single-point displacement meters are arranged in the monitoring section. Among them, the displacement meter at W2 is out of order due to damage and cannot be used. However, based on the displacement change patterns at several other positions and the data from the manual monitoring by the construction unit, it can be inferred that the overall displacement at this point has not changed much, and the slope at this location has remained stable all along. The monitoring results of slope deformation are shown in Figure 4.

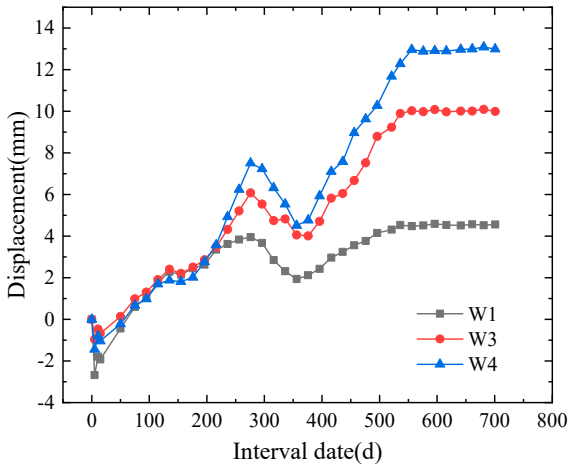

Figure 4. Cumulative displacement curve of the slope surface at each monitoring point.

3.2.2. Investigation of Anchor Cable Axial Forces

In this test, six anchor cables were selected to install the anchor cable dynamometer on the monitoring section, as illustrated by Figure 4. After the M1 was installed, due to

issues in other construction phases, the protective device of the sensor's wire was damaged, causing a malfunction and failure to detect voltage signals. Moreover, some of the wires were pre-buried inside the support structure, making it impossible to repair. In this project, the design lock-off load for the anchor cable is 230 kN. After the actual tension locking, it is found that the anchoring force of each monitoring anchor cable has a certain degree of loss, as illustrated in Table 2.

Table 2. Anchorage force loss of anchor cable after tension locking.

No.	Anchoring Force Locking Value/kN	Locking Loss/kN	Loss Rate %	Loss Value 8 Days After Locking/kN	Loss Rate %	Loss Value 15 Days After Locking/kN	Loss Rate %
M2	204.8	127.6	38.4	−9.6	−4.8	−8.0	−4.0
M3	204.0	99.6	32.8	1.2	0.7	−0.4	−0.2
M4	170.8	52.0	23.3	−14.8	−8.4	6.4	4.1
M5	176.0	55.6	24.0	−10.0	−4.9	−6.4	−3.2
M6	156.8	85.6	35.3	−15.6	−9.4	−28.4	15.9

Locking loss rate = (super tension load-locking load) ÷ super tension load × 100%; loss rate after locking = (locking load-current load) ÷ locking load × 100%.

As illustrated by Table 2, the instantaneous loss of anchorage force after tension locking of each monitoring anchor cable is large, and the loss rate is between 23.3% and 35.3%. In the next two weeks, the anchoring force continues to decrease, but the loss rate decreases. Combined with the on-site construction of the project, the main reasons for the large loss of anchorage force are as follows: (1) the tension operation is not standardized, and the graded tension does not hold, or the holding time is too short during the tension process; (2) the quality of some anchors is not qualified. Following the tensioning of the anchor cable, the clips of some anchors are obviously loose; (3) grouting process problems can be seen. The leakage of slurry during grouting is serious, resulting in poor plumpness of the grouting body in the anchor hole, and the elongation length of the individual steel strands is too large or even pulled out. In addition, stress relaxation of the steel strand and the internal cracks of the slope soil are also the factors that lead to the excessive loss of the anchoring force.

After tensioning and locking, the anchoring force of the cables typically evolves through three stages: accelerated loss, fluctuation change, and continuous stability. The variation trend of the measured anchor cable force in this section is illustrated in Figure 5. Combined with Table 2, it can be seen that due to many on-site influencing factors, after the tension is completed, the acceleration loss of the anchoring force of each monitoring anchor cable in the first stage is mainly concentrated in the unloading stage at the end of tension. As the internal stresses within the slope's rock and soil mass redistribute, the anchoring force experienced the second stage of fluctuating change, which lasted for a long time of about 40 days; after that, the variation in the anchoring force of each cable significantly diminished, and the anchoring force began to rise steadily and lasted for a long time, indicating that during this period, the slope is disturbed by the effect of environmental factors, and the anchor cable continues to play an anchoring role. According to the monitoring data, in the later period, a balance is essentially achieved in the soil–anchor interaction, and the slope stability is good. From the top to the bottom of the monitoring section, the anchoring force of the anchor cable presents a distribution of 'large in the middle and lower part, small at both ends'. The anchoring force of M5 is the largest, which is 288.1 kN, and the anchoring force of M2 is the smallest, which is 239.5 kN.

Comparison of Figures 4 and 5 further reveals that between 230–300 days and 400–560 days, the anchoring force of mid- to lower-slope anchors shows an increasing

trend. Although the increment is smaller than that of the displacement, both exhibit consistent patterns, with M4 and M5 showing the most pronounced increases.

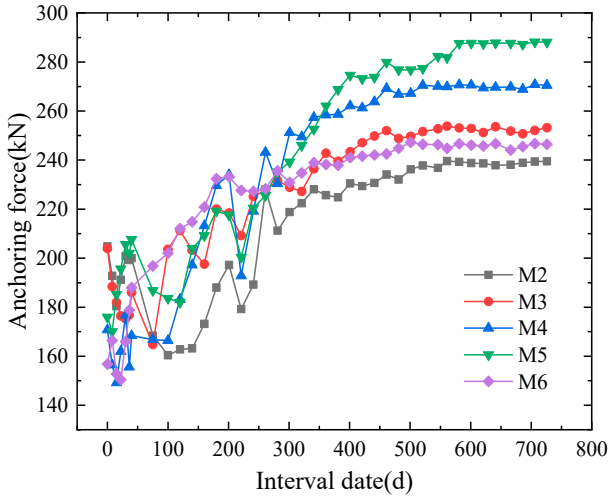

Figure 5. Monitoring anchor cable anchoring force change curve.

4. Establishment and Verification of Finite Element Model

4.1. Establishment of Model

To acquire slope displacement and anchor cable internal force data, PLAXIS 3D is used for modeling and analysis. In the model, the structural members, such as the anchor cable are modeled by the elastic model, and the free section of the anchor cable is simulated by the point-to-point anchor unit; the anchoring section was modeled using an embedded unit, and the slope concrete panel was modeled using a plate unit. The Mohr-Coulomb constitutive model was adopted for soil behavior in the present parametric study because it provides a straightforward, well-established framework compatible with the available in situ shear test data and allows computationally efficient parametric sweeps with PLAXIS 3D, and the soil parameters were obtained from the in situ shear test. Poisson's ratio and the static elastic modulus of the soil were calculated according to the engineering geological manual (fifth edition) [23], which were 0.16 and 2.5 × 104 MPa, respectively. Because the anchor cable spacing is 3 m, an anchor cable spacing is taken as the width of the model. A mesh sensitivity check was performed (coarse, medium, fine meshes) to ensure mesh independence of displacement and anchor forces for the baseline model. The medium mesh used for the parametric study shows variations in <5% in maximum horizontal displacement and <5% in maximum anchor axial force compared to the fine mesh. Boundaries were located sufficiently far from the slope (model length 100 m, height 70 m) to minimize boundary effects; fixed boundary conditions were applied at the bottom and roller boundaries on the lateral sides. Detailed parameters for the retaining structure and the corresponding finite element model are provided in Tables 3–5 and Figure 6, respectively.

Table 3. Material parameters of a free section of bolt.

Member	Tensional Rigidity/kN
Free section	142.0×10^3

Table 4. Material parameters of the anchor bolt anchorage section.

Member	Elastic Modulus	Anchorage Section Diameter/m
Anchorage section	39.0×10^6	0.15

Table 5. Material parameters of the plate element.

Member	Elastic Modulus	Thickness/m
Slope concrete panel	30.0×10^6	0.08

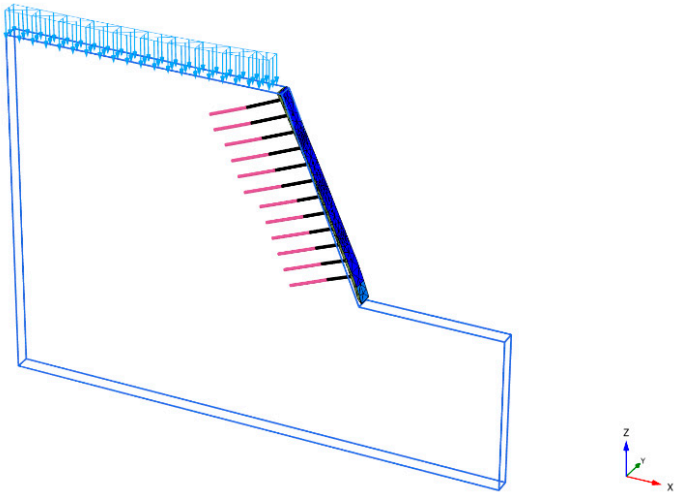

Figure 6. PLAXIS 3D model.

4.2. Comparison of Simulation and Experimental Results

To verify the accuracy of the model and the adopted soil parameters, the calculated slope displacement and the anchoring force from the model (Figure 6) are compared with the field test measurements.

4.2.1. Comparative Analysis of Maximum Lateral Deformation of Slope

As illustrated in Figure 4, the maximum horizontal displacements of W1, W3, and W4 are 4.56 mm, 9.99 mm, and 12.99 mm, respectively. After calculating the slope model, the maximum horizontal displacements of W1, W3, and W4 are 3.46 mm, 8.95 mm, and 12.56 mm, respectively. The comparison results are illustrated in Figure 7. Quantitative agreement between field measurements and the PLAXIS 3D model is summarized using standard error metrics. For the three functioning displacement monitoring points (W1, W3, W4), the simulation yields RMSE = 0.909 mm and MAE = 0.857 mm (average percent error $\approx$ 12.61%), indicating close correspondence in both trend and magnitude. For anchor axial forces (M2–M6), the comparison yields RMSE = 32.64 kN and MAE = 31.10 kN (average percent error $\approx$ 12.17%). These metrics indicate satisfactory agreement for the intended engineering assessments and parametric comparisons described below; local differences (for example, the larger discrepancy at M3) likely arise from local geological heterogeneity, construction practice, and grout quality at the anchor location which are not fully captured by the idealized model, and the results obtained by the finite element model are relatively ideal. However, the maximum horizontal displacement curves of the three monitoring points obtained by PLAXIS 3D-simulated horizontal displacement are consistent with the field-measured horizontal displacement curves. In particular, the two displacement values of the W4 point near the foot of the slope only have a 0.43 mm difference. The above shows the correctness of the calculation model.

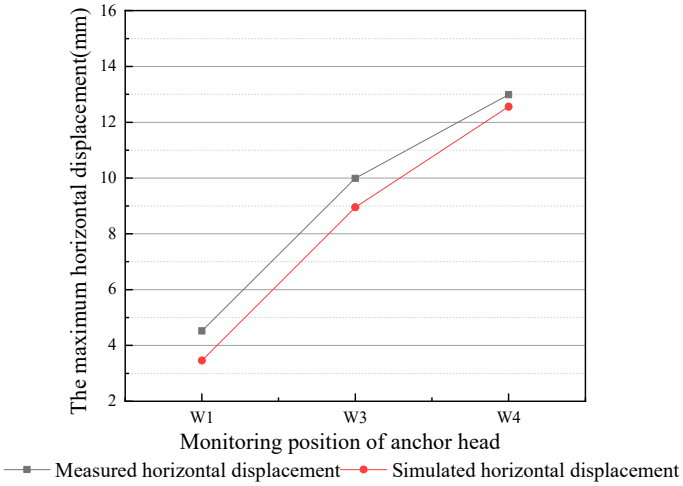

Figure 7. Comparative analysis of slope displacement.

4.2.2. Comparison of Maximum Anchor Cable Forces

As illustrated in Figure 8, the maximum anchoring forces of M2, M3, M4, M5, and M6 monitoring anchor cables obtained by the field test are 239.5 kN, 253.2 kN, 270.5 kN, 288.1 kN, and 246.4 kN, respectively. After calculating the PLAXIS 3D finite element model, the axial forces of M2, M3, M4, M5, and M6 are 199.8 kN, 207.3 kN, 250.3 kN, 262.4 kN, and 222.4 kN, respectively. The comparison of the two results is presented in Figure 8.

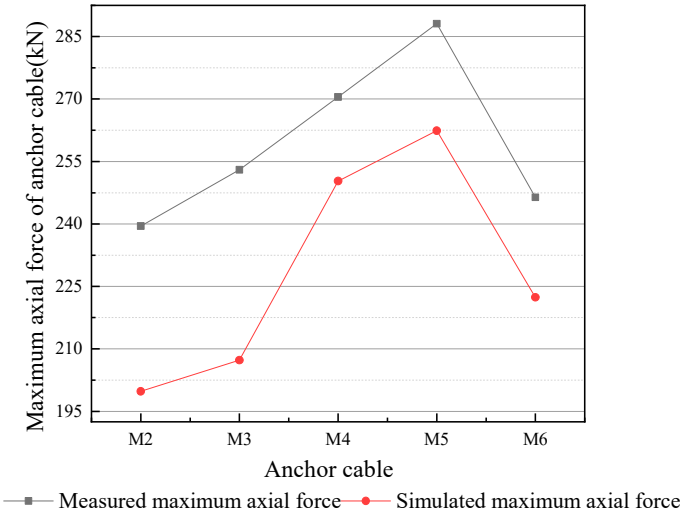

Figure 8. Comparative analysis of anchor cable axial force.

From Figure 8, the axial force of the anchor cable M5 is the largest, indicating that the soil pressure generated by the slope at the M5 anchor cable is the largest. The anchoring force of the anchor cable obtained by the two methods corresponds well with the change in slope height. Because the model establishment conditions are more ideal, the results calculated by the model are less than the field measured results, but the results of each point are about 20 kN. Among them, the larger difference observed at M3 (≈45.7 kN difference) may reflect local differences in anchor quality/grouting, localized soil heterogeneity, or longer-term time-dependent effects (creep or stress redistribution) not captured by the static Mohr–Coulomb model. Follow-up analyses using advanced constitutive models (hardening soil, creep formulations) or additional monitoring (e.g., distributed fiber optic strain) would help assess these mechanisms in more detail.

4.3. Calculated Work Condition

Based on the above analysis, the parameters adopted in the slope finite element model are confirmed to be appropriate and reliable. Therefore, to examine the effect of the number of grades and the width of the platform on the deformation of the slope and the internal force of the anchor cable, and to provide a basis for the reasonable and reliable design of the slope engineering, so as to better guarantee the safety and stability of the slope, based on the original slope finite element model, the number of grades and the width of the platform are changed to study the stability of the high multi-stage slope. In the following research, the slope grading adopts two-level grading and four-level grading, and the platform width selects four widths of 2 m, 3 m, 4 m, and 5 m for finite element simulation and analysis. Platform widths of 2–5 m were selected because they represent typical practical widths for multi-stage slope platforms in similar regional engineering projects given the site constraints (construction access, available bench width, and cost). The parametric framework is readily extensible and can be used to examine larger widths if project conditions allow. The grading and platform width conditions are detailed in Table 6, among which, condition 1 is the original slope condition.

Table 6. Summary of different working conditions of the finite element simulation.

Working Condition	The Slope Order Number	Platform Width
K1	/	/
K2	2	2 m
K3	2	3 m
K4	2	4 m
K5	2	5 m
K6	4	2 m
K7	4	3 m
K8	4	4 m
K9	4	5 m

The parameters for each working condition's finite element model are identical to those of the base case. For the working conditions K2~K8, the GeoStudio 2012 finite element software is used to establish the model, and the overall stability of the slope and the shape of the sliding surface are analyzed. The finite element model was developed using PLAXIS 3D CE V20 software, and the slope displacements as well as anchor cable internal forces under various working conditions were subsequently analyzed.

5. Result Analysis

5.1. Overall Stability Analysis

The slope simulation results were evaluated using the SLOPE/W module within the GeoStudio finite element software, and the slope stability coefficient and the effect range of the sliding surface of the working condition K2~K8 were obtained. The results are detailed in Table 7.

From Table 6, it can be seen that the working condition K1 is the ungraded high slope of the original project, and the working condition K2~K5 is the second-order slope, and the platform width is 2 m, 3 m, 4 m, and 5 m, respectively; and the working condition K6~K9 is the fourth-order slope, and the platform width is 2 m, 3 m, 4 m, and 5 m, respectively. The change in the overall stability coefficient of the slope under each working condition is shown in Figure 9. Combined with Table 7, it is evident that the stability coefficient of the slope increases continuously from working condition K1 to working condition K9, and the slope stability coefficient of working condition K6~K9 increases more significantly. The

analysis confirms that the stability of the slope has been significantly improved, and the more the classification, the larger the width of the platform, and the greater the increase in slope stability coefficient.

Table 7. Stability safety factor and slip surface extent under various working conditions.

Working Condition	Coefficient of Stability	The Distance Between the Entrance of Sliding Surface and the Slope Surface (m)	The Distance Between the Sliding Surface Outlet and the Slope Surface (m)
K1	1.754	27.960	21.037
K2	1.779	27.179	20.816
K3	1.788	26.641	20.663
K4	1.796	26.016	20.437
K5	1.812	25.551	20.389
K6	1.815	25.009	20.277
K7	1.855	23.541	19.923
K8	1.901	22.056	19.556
K9	1.953	20.584	19.174

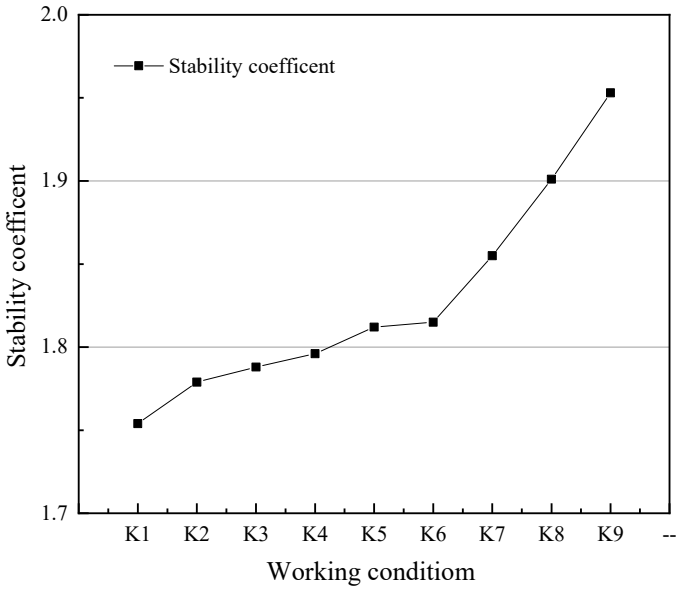

Figure 9. The variation trend of stability coefficient under different working conditions.

5.1.1. Analysis of the Effect of Grading Series on the Overall Stability of the Slope

The stability coefficients of K1, K2, and K6 are shown in Figure 10. For context, the adopted design safety level for the project is the first level. Typical code guidance for permanent cuts often requires factors of safety ~1.5–1.75 (project- and code-dependent). Our baseline case K1 (stability coefficient = 1.754) meets the project's first-level safety requirement; the graded and widened platform cases further improve the margin of safety. Compared with the actual working conditions, the stability coefficient of the slope is increased by about 1.42% by the two-stage slope support. The slope is supported by four levels of slope support, and the stability coefficient is increased by about 3.48%, which is more obvious. The results show that the grading slope support can effectively improve the stability of the slope, and the more the grading, the better the stability.

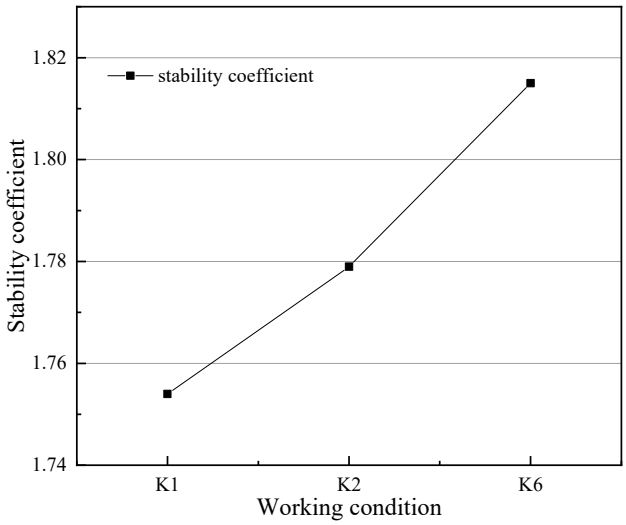

Figure 10. The variation trend of slope stability coefficient under the grading conditions.

5.1.2. Influence of Platform Width on Slope Stability

Under different platform widths, the stability coefficient changes in the two-stage slope support and the four-stage slope support are shown in Figure 11. By analyzing the two-stage slope support and the four-stage slope support, it is evident that the stability coefficient under each working condition increases in proportion to the platform width. In the secondary slope support, with the linear growth of the platform width, the corresponding stability coefficient increases by about 0.68%; in the four-stage slope support, with the linear growth of the platform width, the corresponding stability coefficient increases by about 2.5%. Combined with the analysis of Section 5.1.1, it can be seen that compared to increasing the width of the platform, multi-stage slope support can better improve the stability of the slope when the site conditions permit.

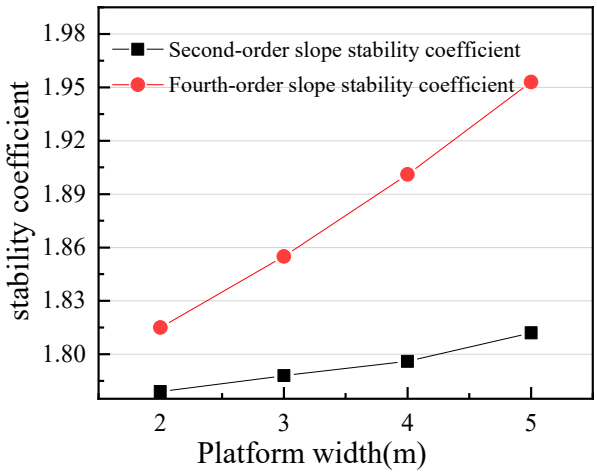

Figure 11. The variation trend of slope stability coefficient under different platform width conditions.

5.2. Analysis of Overall Sliding Surface Range

The relationship between the distance between the exit and entrance of the overall sliding surface and the slope surface under each working condition is shown in Figure 12. Combined with Table 7, it can be seen that with the increase in slope classification and platform width, the distance between the exit and entrance of the overall slip surface of the slope and the slope surface decreases, among which the distance between the entrance of the sliding surface and the slope surface decreases more.

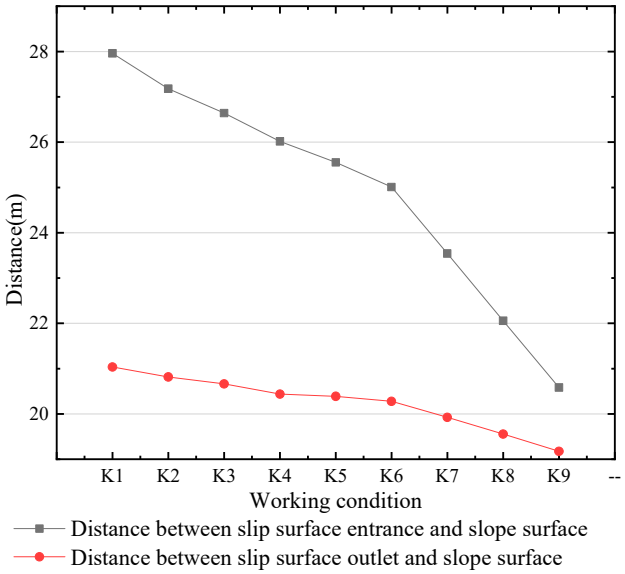

Figure 12. The distance between the entrance and exit of the overall slip surface of the slope and the slope surface under various working conditions.

Analysis of the Effect of Slope Grading Series on the Overall Sliding Surface Range of the Slope

For working conditions of K1, K2, and K6, the distance between the exit, entrance and slope of the overall slip surface of the slope is shown in Figure 13. Combined with Table 7, it can be seen that under these three working conditions, the entrance of the overall slip surface of the slope is 27.960 m, 27.179 m, and 25.009 m from the broken surface, respectively, and the exit of the overall slip surface of the slope is 21.037 m, 20.816 m, and 20.277 m from the broken surface, respectively. With the increase in slope grade, the distance between the exit and entrance of the overall slip surface of the slope and the slope surface decreases. Compared with the entrance of the overall sliding surface, the exit position shows a more significant reduction in its distance from the slope surface. Specifically, relative to the original condition, the range of influence of the entrance of the overall slip surface decreases by nearly 3 m, indicating a notable effect.

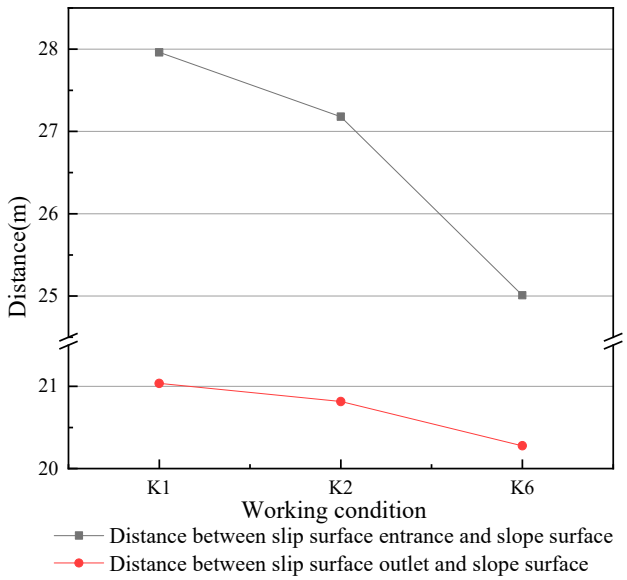

Figure 13. The distance between the entrance and exit of the overall slip surface of the slope and the slope surface under the grading conditions.

5.3. Slope Displacement Analysis

5.3.1. Analysis of Horizontal Displacement Distribution of Single-Stage Slope

The distribution of horizontal displacement along the height of the original slope is presented in Figure 14. Following the completion of slope cutting and support measures, the displacement at various positions initially increases and then decreases with increasing elevation. The displacement peaked near one-tenth of the slope height above the slope toe (≈9.73 mm), suggesting a likely potential slip surface in that zone. However, it should be noted that acceptable displacement thresholds are project-specific and depend on design criteria and structural tolerance, which must be defined in accordance with project requirements.

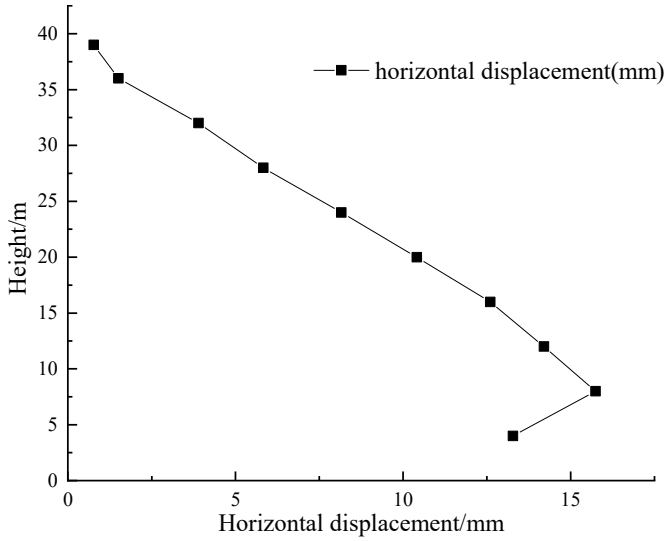

Figure 14. Horizontal displacement distribution of slope at different heights.

5.3.2. Analysis of the Effect of the Slope Level on the Horizontal Displacement of the Slope

In this section, when the working condition K1 is graded, the width of each platform is selected to be 2 m. Figure 15 is the horizontal displacement cloud diagram of the finite element analysis of the original engineering slope, the second-stage slope, and the fourth-stage slope. As shown in Figure 15, the greatest displacements of the original slope and the second-stage slope with a platform width of 2 m are 15.74 mm and 13.46 mm, respectively. In contrast, it is reduced by 2.28 mm and 14.48%, indicating that slope grading effectively mitigates the development of horizontal displacement. For the four-stage slope with a 2 m width, the peak displacement is 11.95 mm, which is 1.51 mm less than that of the two-stage slope, which is reduced by 11.22%. The above fully shows that slope grading enhances slope stability, and the more grading, the more favorable; this is to ensure the stability of the slope.

5.3.3. Platform Width and Its Effect on Slope Horizontal Displacement

As illustrated in Figure 16, when the platform width is 2 m, 3 m, 4 m, and 5 m, for the secondary slope, the maximum horizontal displacement values are 13.46 mm, 13.36 mm, 13.10 mm, and 12.56 mm, respectively. Results indicate that the maximum horizontal displacement of the secondary slope decreases progressively with increasing platform width. For the secondary slope, the maximum horizontal displacement of the slope is reduced by 0.1 mm, 0.26 mm, and 0.54 mm, respectively, which is reduced by about 0.74%, 1.9%, and 4.1%, respectively. This phenomenon indicates that increasing platform width contributes positively to slope stability, with larger widths producing more pronounced effects.

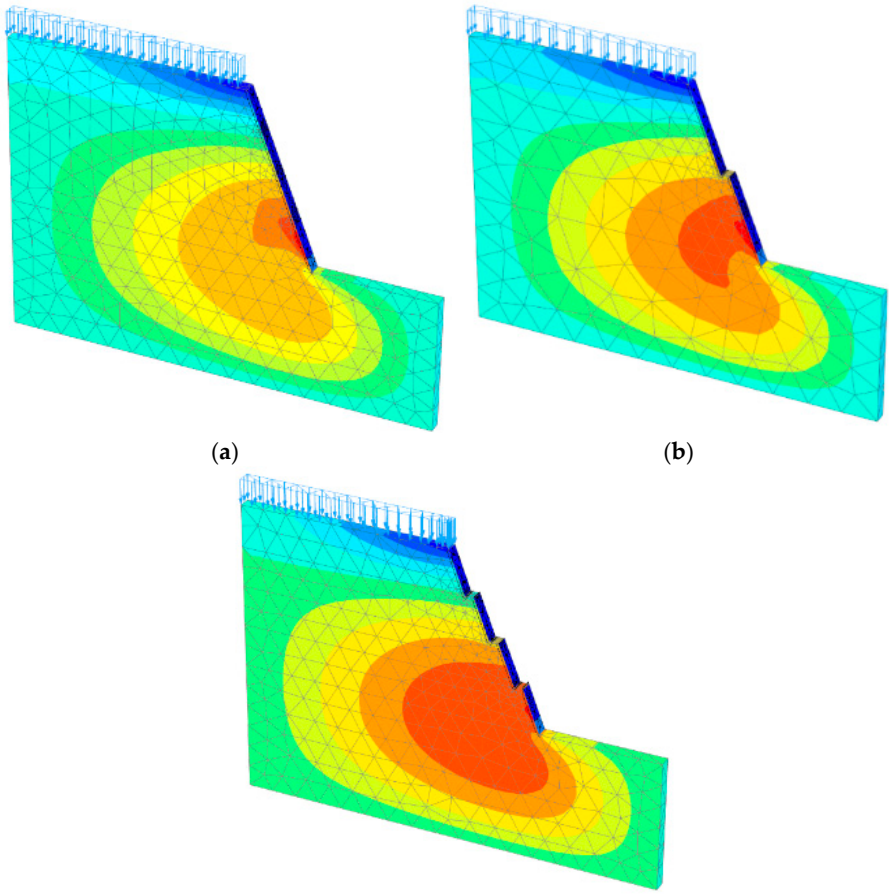

Figure 15. Horizontal displacement cloud diagram of slope at all levels: (**a**) the horizontal displacement cloud diagram of the original engineering slope; (**b**) horizontal displacement cloud diagram of secondary slope; (**c**) horizontal displacement cloud diagram of four-level slope.

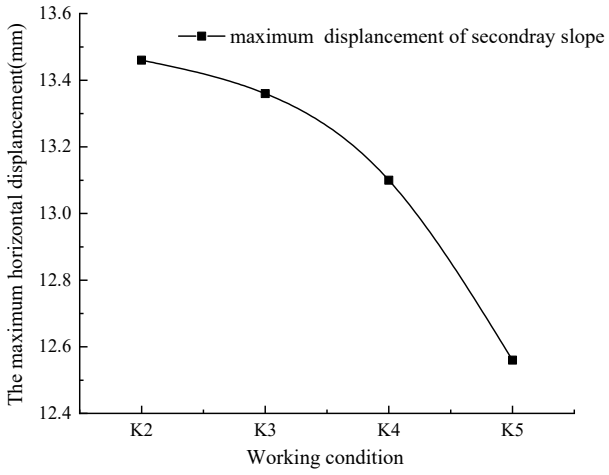

Figure 16. Horizontal displacement of secondary slope under different platform widths.

The maximum horizontal displacement of the slope under different platform widths is shown in Figure 17. When the platform widths are 2 m, 3 m, 4 m, and 5 m, respectively, the maximum horizontal displacements of the four-stage slope are 11.95 mm, 11.78 mm, 10.51 mm, and 10.03 mm, respectively. Under each working condition, the maximum horizontal displacement of the slope is reduced by 0.17 mm, 1.27 mm, and 0.48 mm, respectively, which is reduced by about 1.4%, 10.78%, and 4.5%, respectively. These findings

show that slope stability improves with increased platform width. In the case of the four-level slope, the 4 m platform width produces the largest decrease in horizontal displacement, differing from the two-level slope but without altering the overall stability trend.

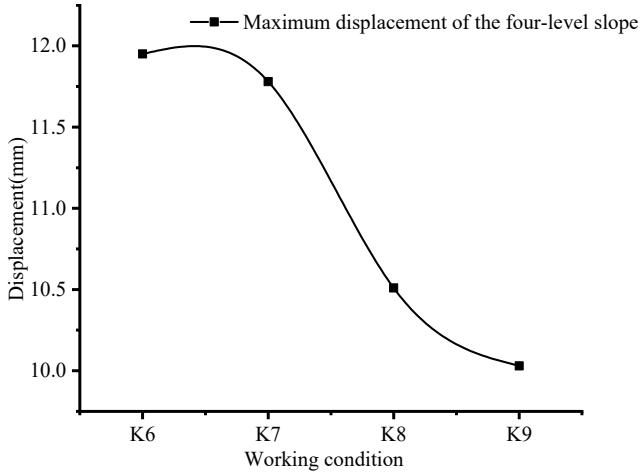

Figure 17. The horizontal displacement of the four-level slope under different platform widths.

5.4. Axial Force Analysis of Anchor Cable

5.4.1. Analysis of the Effect of Single-Stage Slope Anchor Cable Axial Force

The distribution of maximum axial forces for each row of anchor cables in the original slope is illustrated in Figure 18. As shown, the axial forces are relatively uniform, with only minor differences between the first and last rows. From top to bottom, the maximum axial force gradually decreases, reaching the lowest value of 199.8 kN in the fourth row. However, starting from the seventh row, the axial force increases sharply, peaking at 269.7 kN in the ninth row. Beyond the tenth row, the axial force again decreases, with the twelfth row approaching the design anchorage force value. This distribution pattern arises mainly because earth pressure is concentrated in the middle and lower parts of the slope, causing anchors in these zones to bear greater loads. In contrast, due to the relatively high shear strength of the soil and the inherent stability of the slope, axial forces in the middle–upper anchors remain below the design values, and the effects of groundwater and seepage were not considered, resulting in partial underutilization of these anchors. In general, the change in axial force in each row of anchor cables simulated by the finite element method is consistent with the distribution of field measurement results.

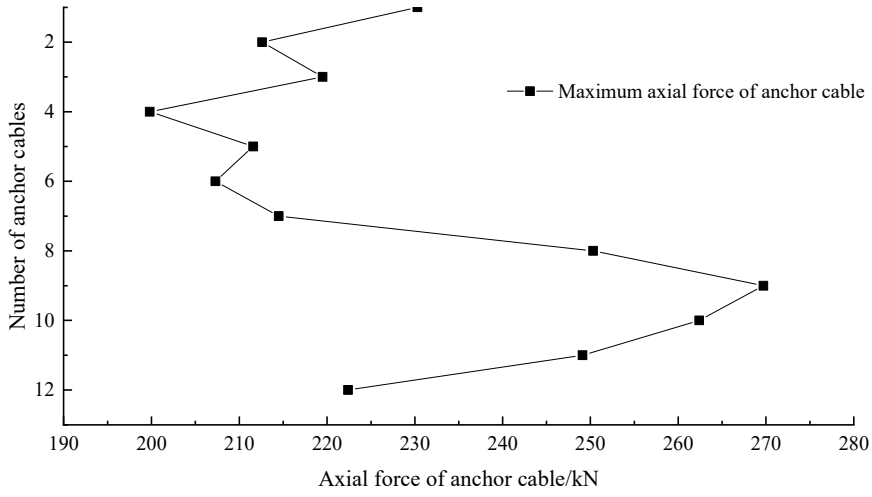

Figure 18. The maximum axial force distribution map of each row of anchor cables in the slope of the original project.

5.4.2. Analysis of the Effect of Slope Series on the Axial Force of Anchor Cable

The variation curves of the maximum axial forces for each row of anchor cables under different slope grading conditions are presented in Figure 19. As shown in Figure 19, increasing the number of slope levels leads to a reduction in axial forces across all anchor rows. For the upper–middle portion of the slope, the two-level grading provides the most significant reduction, lowering axial forces by approximately 9.5%. In the middle–lower portion, the axial forces gradually decrease with additional grading, with the four-level slope yielding the most pronounced reduction, lowering the maximum axial force by about 27%. Overall, compared with the original single-level slope and the two-level slope, the four-level configuration exhibits the lowest axial forces across all anchor rows. These findings indicate that increasing slope grading effectively reduces the required design anchorage force of the cables, with the effect becoming more evident as the number of levels increases. In this project, the most substantial reductions occur in the fourth and tenth rows of anchor cables.

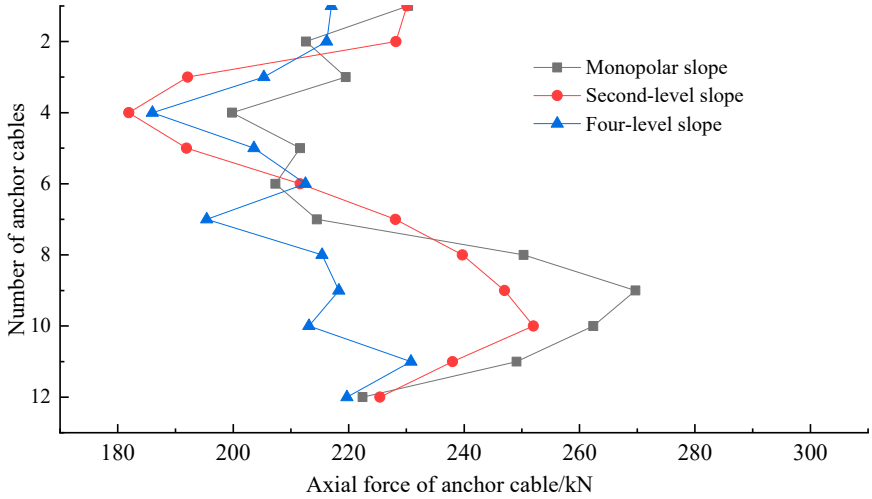

Figure 19. The maximum axial force distribution diagram of each row of anchor cables under different slope grades.

5.4.3. Analysis of the Effect of Platform Width on the Axial Force of Anchor Cable

In this section, the distribution results of the axial force of the anchor cable with different platform widths are taken when the second-level slope and the fourth-level slope are taken, respectively, and the effect of the width of each platform and the axial force of the anchor cable under different slope stages is analyzed.

(1) The effect of different platform widths on the axial force of anchor cable under second-level slope

According to Table 6, the second-level slope was evaluated with platform widths of 2 m, 3 m, 4 m, and 5 m, and the corresponding maximum axial force distributions of the anchor cables are illustrated in Figure 20. As shown in the figure, variations in platform width exert minimal effect on the axial forces of the upper–middle anchor rows. In contrast, for the middle–lower anchors, increasing platform width leads to higher maximum axial forces. When the width is 5 m, the maximum axial force of the eighth-row anchor reaches 276.8 kN, whereas at a width of 2 m, it is only 255 kN. Overall, for the second-level slope, the effect of platform width on anchor axial force distribution is relatively minor.

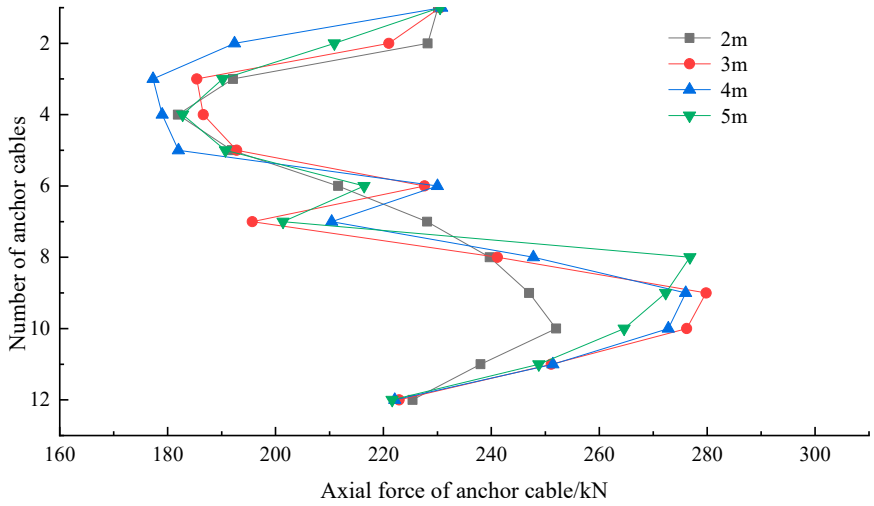

Figure 20. The maximum axial force distribution diagram of anchor cable under different platform widths of the secondary slope.

(2) The effect of different platform widths on the axial force of the anchor cable under fourth-level slope

According to Table 6, the fourth-level slope was analyzed with platform widths of 2 m, 3 m, 4 m, and 5 m, and the corresponding maximum axial force distributions of the anchor cables are illustrated in Figure 21. As illustrated, the distributions for the 2 m and 3 m platforms are generally consistent, though minor differences exist. For the upper anchor rows, the axial forces reach their highest values when the platform width is 4 m. For the lower anchors, the axial forces remain similar across the 2 m, 3 m, and 4 m cases, but when the platform width increases to 5 m, a significant reduction occurs, with the maximum decrease reaching approximately 11%. Overall, for the fourth-level slope, the effect of platform width on the axial force distribution of anchor cables does not exhibit a clear or uniform trend.

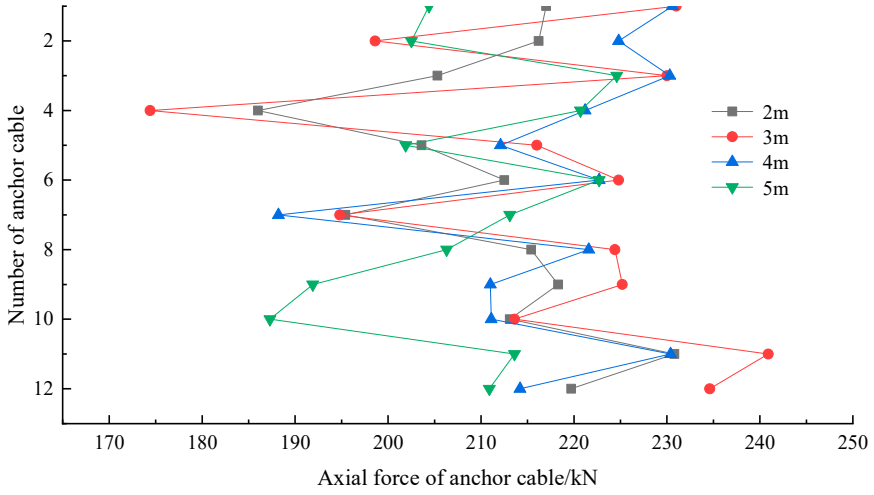

Figure 21. The maximum axial force distribution diagram of the anchor cable under different platform widths of the four-stage slope.

6. Conclusions

Based on the engineering example, through field monitoring tests and finite element simulations, this paper explores how the number of slope classifications and platform width affect slope stability, horizontal displacement, and anchor cable axial force. The principal conclusions are outlined below:

(1) The establishment of remote wireless monitoring and the data automatic acquisition system, as well as timely analysis of the monitoring data, through real-time monitoring of the stability of the slope operation stage, prevents slope instability in advance. It is found that the change in the anchoring force of anchor cable of the displacement meter at each monitoring point has tended to be stable. A maximum displacement of 12.99 mm is recorded at the lower part of the slope, and the peak anchoring force of 288.1 kN is observed in the middle to lower section. Combined with on-site inspection, the slope has been in a stable state in the operation stage and has good stability. Earth pressure and sliding block geometry concentrate lateral loads in the mid-to-lower portion of the slope; thus, anchors located in these areas intercept higher active pressures. The lever arm and the geometry of the mobilized slip mass explain the observed distribution of axial forces along the anchor rows. Grading reduces the size/height of an individual sliding block and redistributes stresses.

(2) The findings show that combining multi-stage slopes with frame prestressed anchor cables yields greater stability than direct support and increases the slope stability coefficient. Compared with increasing the width of the platform, increasing the number of slope grades is more effective in enhancing slope stability. The distance between the entrance and exit of the overall slip surface of the slope and the slope surface will also decrease with the increase in the slope classification and the width of the platform. If the site conditions permit, increasing the classification can reduce the distance between the entrance and exit of the overall slip surface of the slope and the slope surface, thus greatly increasing overall slope stability.

(3) The study on the horizontal displacement of the slope shows that the horizontal displacement of the slope reaches the maximum near the bottom of the slope under the conditions of grading and changing the width of the platform. With the increase in the grade and the width of the platform, it is helpful to reduce the horizontal displacement of the slope. Both of these factors strongly affect the horizontal displacement, and their joint effect on slope deformation must be taken into account during the design process. The observed reduction in maximum anchor axial force with increased grading (up to ≈27% reduction in our parametric cases) implies potential for optimized anchor prestress and length selection when grading is feasible; however, safety factors, construction tolerances, and grout quality must be included in final designs.

(4) The axial force of the anchor cable is basically close to the prestress of anchor cable. Through the study, it is found that the finite element simulation value of the axial force of each row of the anchor cable in the slope is not much different from the measured results, and the distribution along the slope height is also consistent. Increasing the number of slope classifications will reduce the maximum axial force. The more the classifications, the smaller the axial force, which can reduce the design value of the anchor cable anchoring force. Increasing the number of grades has the most effective effect on reducing the axial force of the fourth and tenth rows of anchor cables; the effect of increasing the width of the platform on reducing the axial force is not obvious.

Author Contributions: Conceptualization, J.L. and S.Y.; methodology, J.L. and S.Y.; resources, J.L., S.Y., N.L. and B.L.; data curation, J.L., N.L. and B.L.; writing—review and editing, J.L.; visualization, J.L. and N.L.; supervision, J.L. and Y.Z. All authors have read and agreed to the published version of the manuscript.

Funding: Gansu Province Science and Technology Plan Project (24JRRA292); the Gansu Province Young Talents (Team Project) of CPC Gansu Provincial Committee Organization Department (No. 2025QNTD09); Gansu Province Higher Education Teacher Innovation Fund Project (2025B-242); the National Natural Science Foundation of China (52168050).

Data Availability Statement: The data that support the findings of this study are available from the corresponding authors upon reasonable request.

Acknowledgments: The authors acknowledge support from the Lanzhou Institute of Technology, and the Lanzhou University of Technology.

Conflicts of Interest: The authors declare no conflict of interest.

References

1. An, B.; Wang, C.; Liu, C.; Li, P. A multi source remote sensing satellite view of the February 22nd Xinjing landslide in the mining area of Alxa left Banner, China. *Landslides* **2023**, *20*, 2517–2523. [CrossRef]
2. Ozbay, A.; Cabalar, A.F. FEM and LEM stability analyses of the fatal landslides at Çöllolar open-cast lignite mine in Elbistan, Turkey. *Landslides* **2015**, *12*, 155–163. [CrossRef]
3. Yin, Y.; Huang, B.; Chen, X.; Liu, G.; Wang, S. Numerical analysis on wave generated by the Qianjiangping landslide in Three Gorges Reservoir, China. *Landslides* **2015**, *12*, 355–364. [CrossRef]
4. Belloni, L.G.; Stefani, R. The Vajont slide: Instrumentation—Past experience and the modern approach. *Eng. Geol.* **1987**, *24*, 445–474. [CrossRef]
5. Zhang, H.; Wu, R.; Zheng, Y.; Wang, R.; Wei, J. Study on pile-anchor supporting effect of multi-stage cutting high slope based on FLAC3D-Taking a landslide in Yunnan as an example. *J. Chongqing Jiaotong Univ. Nat. Sci. Ed.* **2024**, *43*, 28–38.
6. Wu, H.; Sun, M.; Wang, J. Stability Assessment of Multi-Stage Slopes Considering Local Failure. *Front. Earth Sci.* **2022**, *10*, 798791. [CrossRef]
7. Yu, Z.; Dong, D.; Jiang, Y.; Chen, G.; Huang, Q. Research on optimization design of soft soil subgrade and high slope based on numerical simulation-Taking a subway parking lot as an example. *Exp. Technol. Manag.* **2025**, *42*, 165–173.
8. Yang, Z. Simulation study on high slope stability based on creep test. *J. Xi'an Univ. Sci. Technol.* **2023**, *43*, 988–999.
9. Zhou, C.; Dong, X.; Li, Z.; Ma, Z. Analysis of the effect of rainfall infiltration on the stability of multi-stage slope reinforced by anchor rod. *Sci. Technol. Eng.* **2022**, *22*, 12550–12556.
10. Zhu, X.; Shao, S.; Shao, S.; Ji, Y.; Yu, Z. Pseudo-dynamic analysis of three-dimensional soil slope stability based on nonlinear criteria. *Chin. J. Geotech. Eng.* **2025**, *47*, 1925–1935.
11. Li, J.; Ye, S.; Cui, X.; Liu, B.; Li, N. Displacement Calculation of a Multi-Stage Homogeneous Loess Slope Under Seismic Action. *Buildings* **2025**, *15*, 1484. [CrossRef]
12. Jia, G.; He, J.; Yu, J.; Zhao, L.; Pan, Q. Dynamic stability analysis of a three-stage slope under random ground motion effect. *J. Guangxi Univ. Nat. Sci. Ed.* **2024**, *49*, 1235–1243.
13. Luo, W.; Liu, S.; Xu, C.; Chen, J.; Lu, Q. Quasi-static limit upper bound analysis of seismic stability of multi-stage slopes. *Earthq. Disaster Prev. Technol.* **2024**, *19*, 810–820.
14. Yan, C.; Wang, H.; Cao, J.; Kang, W.; Li, Q. Upper bound solution for stability analysis of loess heterogeneous multi-stage high slope. *J. Wuhan Univ. Eng. Ed.* **2025**, *58*, 397–406.
15. Li, J. The safety control mechanism of wide platform on the stability of high cutting slope. *J. Xi'an Univ. Sci. Technol.* **2022**, *42*, 1163–1171.
16. Jia, Z. Stability analysis of high slope supported by frame anchor under freeze-thaw cycle load. *Highway* **2025**, *8*, 38–44.
17. Zhao, C.; Fan, Z.; Ran, L.; Zhou, F.; Tan, W. Construction technology of anchor cable anchor frame beam support in broken rock and soil high slope. *Highway* **2023**, *68*, 50–53.
18. Zhu, Y.; Wei, Z.; Yang, X.; Zhu, Q. Monitoring and analysis of multi-stage high fill slope supported by prestressed anchor cable pile-slab wall. *China Rural. Water Conserv. Hydropower* **2020**, *7*, 202–207.
19. Wang, D.; Wu, Z.; Zhang, J.; Jiang, Y. Analysis of the effect of multi-stage composite support structure on the seismic performance of heterogeneous high slope. *J. Vib. Eng.* **2019**, *32*, 404–414.
20. Wang, J.; Liu, S.; Pu, X.; Zhao, R. Reliability and sensitivity analysis of loess high slope stability under lattice bolt support. *Math. Pract. Underst.* **2020**, *50*, 186–194.
21. Li, J.; Zhu, Y.; Ye, S.; Ma, X. Experimental study and analysis on health monitoring of a secondary high slope. *J. Geotech. Eng.* **2018**, *40*, 129–134.
22. Ye, S.; Shi, Y.; Gong, X.; Chen, C. Numerical analysis of seismic response of multi-stage high slope reinforced by frame prestressed anchor. *J. Geotech. Eng.* **2018**, *40*, 153–158.
23. Hua, J.; Zheng, J. *Engineering Geological Handbook*, 2nd ed.; China Construction Industry Press: Beijing, China, 2018; pp. 174–179.